Equation of state of colloids coated by polyelectrolyte multilayers

Monique Dubois,[1,2] Monika Schönhoff,[3,*] Annette Meister,[2] Luc Belloni,[2]
Thomas Zemb,[2] and Helmuth Möhwald[1]
[1]*Max-Planck Institute of Colloids and Interfaces, D-14424 Potsdam/Golm, Germany*
[2]*CEA Saclay: DSM/DRECAM/SCM/LIONS, 91191 Gif sur Yvette cedex, France*
[3]*Institut für Physikalische Chemie, Westfälische Wilhelms-Universität Münster, Corrensstraße 30, D-48149 Münster, Germany*
(Received 20 April 2006; revised manuscript received 29 August 2006; published 8 November 2006)

We propose an adaptation of the osmotic stress technique for determining equations of state of colloids covered by polymer films. We describe here the case of silica particles covered by 6 or 7 layers of polyelectrolyte multilayers. The establishment of a pressure-distance curve allows the interpretation of colloidal interactions over more than four orders of magnitude in pressure. This large range allows a clear separation between three distinct regimes: layer compression, brush extension and at very low pressures a regime of weak repulsion. The physical origins of the regimes are discussed and described by models of colloidal interactions.

DOI: 10.1103/PhysRevE.74.051402 PACS number(s): 82.70.Dd, 81.16.Dn

I. INTRODUCTION

The equation of state of a complex fluid is the relation between osmotic pressure, temperature and molar volume, i.e. the volume occupied by a mole of colloids. The experimental determination requires precise measurement of the three quantities on the same sample. The equation of state contains all information about colloidal interactions, since osmotic pressure, minus the derivative of free energy versus volume, can be calculated from any theoretical model and used to experimentally test the predictive power of models of forces in soft condensed matter. The simplest is the perfect gas model, demonstrated to be valid by Van't Hoff for solutions. The second general model used is the van der Waals fluid, with a covolume and a correction due to attractive interactions. The first experimental determination of the Avogadro number N_A was done by Jean Perrin in his classical work on the sedimentation of colloids—analogue to an "atmosphere" of particles—using a monodisperse emulsion of vegetal gum below glass transition temperature [1]. A more quantitative determination was then achieved at the beginning of the XXth century by Jean Perrin using a monodisperse sample, where the monodispersity required for a determination of N_A with a few percent precision was obtained after seven fractionations induced by depletion and recrystallization. Since these pioneering times, equations of state of other colloids were established: inorganic nanoparticles by the Utrecht school under impulsion of Overbeek [2], bilayers of phospholipids by Parsegian and co-workers [3], DNA by Podgornik [4]; the equation of state of synthetic clay particles such as laponite is only known since a few years [5]. The equation of state of diluted colloidal crystals [6] as well as of glycolipids [7,8] has recently been measured and confronted to modern theories of intermolecular interactions. While osmotic stress equilibration has been employed to obtain these equations of state, analytical centrifugation is an alternative method [9,10], as it enables to obtain a complete equation of state in one sample by extracting the particle density as a function of position and rotational speed. In order to obtain a good discrimination between predictive models of molecular forces, the equation of state has to be determined over the largest dynamical range possible.

A largely studied new type of particles of colloidal dimensions is the polyelectrolyte microcapsule. These materials are obtained by a controlled layer-by-layer technique [11] described in recent reviews [12–14]. The first layer is deposited on a "core," which can be made of different types of solid particles (from a living cell to silica nanoparticles or decomposable polymer), which can finally be dissolved [15]. Hollow microcapsules prepared in this way are novel approaches in encapsulation [16], drug delivery [17], nanoreactors [18] or, after compaction, in innovative material design, such as photonic crystals [19]. Handling of such microcapsules, a type of colloids known and mastered for less than ten years, requires a good knowledge of mechanical properties of this hollow material [20], as well as the different possible interaction mechanisms between capsules.

At first glance, these are deformation of the polyelectrolyte multilayer (PEM), interpenetration of outer layer extended segments, uncompressed contact between non-interdigitated outer layer segments and electrostatic interaction between well-separated charged colloids. Several studies have dealt with force measurements on such multilayers on surfaces, employing local techniques, which apply to a certain range of forces [21,22]. Measuring colloidal forces with osmotic pressure is known to have a larger dynamic range and a greater sensitivity than experiments using surface force apparatus (SFA) [23–26] or the colloidal probe version of AFM [27,28].

The aim of this work is to provide a universal approach, establishing experimentally the equation of state of polymer-coated colloids from dense packing to dilute solutions, and identifying different regimes dominated by different types of repulsive forces—crucial for understanding colloidal stability.

*Corresponding author. FAX +49-251-8329138. Email address: Schoenho@uni-muenster.de

II. EXPERIMENTAL

A. Materials

The polyelectrolytes used throughout this work are poly (diallyl dimethylammonium chloride) (PDADMAC, $M_w \sim 100000-150000$) and poly (allylamine hydrochloride) (PAH, $M_W \sim 70000$) as polycations, and poly (styrene sulfonate sodium salt) (PSS, $M_W \sim 70000$) as polyanion. All polyelectrolytes are purchased from Aldrich Chemical Co. PDADMAC and PAH are used without further purification, whereas PSS is dialyzed against ultra pure water (cut-off of $M_w > 14000$), and subsequently lyophilized. The water used in all preparation procedures is purified with a three-stage purification system (Seradest) and has a resistivity higher than 18.2 MΩ cm. Monodisperse silica particles with a nominal diameter of 300 nm are obtained from Geltech Inc. The powdered silica is dispersed in pure water and washed in centrifugation-decant-redispersion steps until the measured ζ-potential is stable.

B. Preparation methods

1. Polyelectrolyte multilayers

The polyelectrolyte multilayers are prepared using a method first described by Sukhorukov *et al.* [29], which was further optimized for coating high concentrations of small ($<\mu$m) colloidal substrates [30]: Here, 80 ml of a silica colloid dispersion (2.5% wt, salt free) is added drop wise into 200 ml of a concentrated (1.5 mg/mL) polymer solution, containing 0.5 M NaCl. The dispersions are filled up to 400 ml with ultra pure water and left for an adsorption time of 15 min. Following that, the colloids are washed in repeated centrifugation-decantation-redispersion steps using pure water until the ζ-potential of the colloids reaches a stable value and the resistivity of the decanted solution is in the MΩ/cm range.

As a first layer, PDADMAC is adsorbed, then the process is repeated alternatingly with PSS or PAH until six or seven, respectively, single layers are obtained. Alternatively to PAH, a part of the samples is terminated by PDADMAC as the 6th layer. After each deposition the Zeta potential is monitored in dilute dispersions using a Zeta-Sizer 4 (Malvern), furthermore single particle light scattering (SPLS) is used to verify that the particles remain monodisperse and do not aggregate.

2. Purification of dispersions

Imposing a controlled osmotic stress without salt requires starting from salt-free solutions where the conductivity is lower than 10 μS. Colloidal dispersions are washed several times. Water is added to the solution. Phase separation in the form of sedimentation occurs after several days, depending on salt concentration. Sedimentation is driven by the high particle density and by the screening of Coulomb repulsion in salt solution. At that point, one can remove the supernatant solution. One repeats this experiment until sedimentation appears very slowly and conductivity is low. The last purification is achieved by dialysis in a bag of regenerated cellulose with a nominal cut-off 100 000 Daltons (spectra/Por CE Float-A-Lyser, diameter 10 mm, Volume 3 mL) in order to ensure that polyelectrolytes which are not attached on the capsules are not present in the solution. In the reservoir, "double bed" resin (cationic+anionic resins) is added to enhance salt extraction. This resin allows maintaining a very low conductivity in the reservoir (<1 μS). Adding mixed bed resin in the reservoir ensures the concentration of residual salt in the capsule solution to decrease faster because ions leaching are immediately exchanged versus H^+ or OH^-. Finally, salt-free dispersions of a concentration of 10% (vol) particles are obtained.

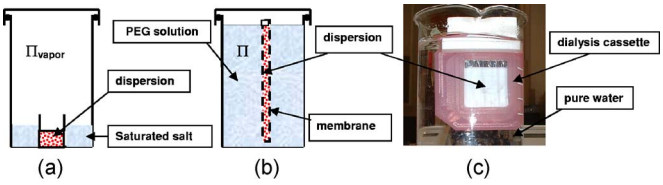

FIG. 1. (Color online) Osmotic pressure equilibration in different pressure regimes. (a) Vapor pressure, (b) dialysis via membrane, and (c) sedimentation

C. Osmotic stress equilibration methods

Osmotic pressure is imposed onto the dispersions using different methods, as shown in Fig. 1. For pressures above 10^5 Pa vapor pressure equilibrium against saturated salt solutions is employed [see Fig. 1(a)], whereas for lower pressures the colloidal dispersion is put in contact with aqueous polymer solutions through a membrane [Fig. 1(b)].

1. Dialysis

This method is used to impose pressures less than 10^5 Pa, see Fig. 1(b). The colloidal dispersion is put in contact with aqueous polymer solution (dextran 110 000 or PEG 20000) via a dialysis membrane (Slide-A-Lyser dialysis cassette 0.5–3 mL 35 000 Daltons Pierce). The volume of the dispersion must be several orders of magnitude lower than that of the polymer solution to avoid variations in concentration during equilibration. At the end, the particle dispersion has the same osmotic pressure than the stressing polymer solution in the reservoir. Dialysis cassettes are closed by a septum and immersed into the reservoir. To equilibrate the hydrostatic pressure induced by membrane stretching between the reservoir and the sample contained in the cassette, an open hypodermic needle is introduced into the septum to allow equilibration via atmospheric pressure. The reservoir is closed to avoid evaporation. During the course of equilibration, dispersion had to be added due to the loss of volume caused by compression. One month is typically needed for osmotic equilibrations when polymer solutions are viscous. When equilibrium is achieved, the concentration of water is measured by the Karl Fischer titration method (Coulometer Metrohm 684KF, Swiss) analyzing the concentration of water using the following procedure: a known volume of the equilibrated sample is extracted and introduced in a known volume of dry ethanol, then dispersed by ultrasonic treatment

and centrifuged to remove capsules from the alcohol/water solution.

2. Vapor pressure

To impose osmotic pressures higher than 10^5 Pa, osmotic stress control via polymer solutions is not appropriate, since too high polymer concentrations would be required, leading to very viscous solutions, where equilibrium is obtained too slowly. The method used for high pressures is vapor pressure equilibrium [31], see Fig. 1(a):

In a closed box, a sample is introduced in contact to vapor pressure regulated by a saturated salt solution. Water vapor pressures P of several saturated salts are tabulated [31], and the osmotic pressure can be deduced from the relation:

$$\Pi = -\frac{kT}{v}\ln\left(\frac{P}{P_0}\right), \tag{1}$$

where $kT=4.12\times10^{-21}$ J at room temperature and $v=30\times10^{-24}$ cm^3 is the molecular volume of water [23]. P_0 is the saturation vapor pressure (alias 100% humidity) for the pure solvent at the same temperature and P the pressure measured above the solution, which contains excess salt in the crystalline state. The concentration of water in the final particle dispersion is measured in the same way as described above.

Finally, it must be noted that towards high-pressure values osmotic stress experiments are only limited by the possible value of the vapor pressure. If the water vapor activity is low, evaporation is occurring limited by capillary condensation. The maximum radius of vapor bubbles R_b, which could form between four adjacent spheres of radius R_s can be estimated to ($R_b=R_s/10=14$ nm). Using the Kelvin-Laplace relation giving the excess hydrostatic pressure of a fluid with surface tension versus the vapor:

$$P_L = 2\gamma/R_b, \tag{2}$$

We find for 100% water activity an upper limit of possible pressures to be measured of 10^7 Pa. Since the water activity is reduced by the presence of the PEM, the effective upper limit is even somewhat higher, and estimated to be of the order of 10^8 Pa. An understanding of the behavior of a dried outer layer is also important for practical purposes, such as slow drying, atomization or possible re-swelling of the dry material [32]. Indeed, when trying to measure higher stresses using $K_2Cr_2O_7$ as desiccating salt (98% of relative humidity [31]), a dry non-redispersable paste is produced from the PEM covered silica dispersion used in this work. In practical applications such as paints, covered with polyelectrolyte layers, the equation of state allows thus to identify the pressure at which weight loss due to nucleation of bubbles in the holes between compacted solid particles become relevant.

D. Analytical methods

1. Chemical analysis

By quantitative analysis of the elements (Si, C, N) contained in the sample one can extract the silica/polyelectrolyte ratio. The layer series PDADMAC/PSS/PAH/PSS/PAH/PSS/PAH$^+$ coated onto SiO_2 is analyzed (Analytische Laboratorien, D-51789 Lindlar, Germany). The average carbon to silica ratio m_C/m_{Si} from several samples is 0.1, while the nitrogen data scatter too much for a quantitative analysis. Taking into account the monomer masses of the different polyelectrolytes and assuming a stoichiometric ratio of the structural charges in subsequent layers of 1:1, the total polymer coverage is calculated to 12 mg/m^2. For the terminating PAH layer, neglecting Manning condensation, this results in a charge density of 14 μmol m^{-2}. With half of the charges needed to neutralize the charge of the preceding layer, the excess surface charge is 7 μmol m^{-2}, which results in 1.2 10^6 charges per colloid.

2. Determination of the water content

A small amount of dispersion equilibrated at defined osmotic pressure is weighed and added to a known volume of dry ethanol. Then the concentration of water in the sample is obtained by a classical Karl Fisher experiment. The water content in the third regime is directly determined via the density of the liquid sample, using a high precision (six digits) diapason temperature-controlled densitometer manufactured by Anton Paar ref DMA 5000.

E. USAXS measurements

The ultra-small-angle x-ray scattering (USAXS) measurement has been performed on a home-made instrument able to record full small angle X-ray scattering curves in the range from the standard q-range of light scattering to X-ray crystallography [33] on absolute scale, i.e; determining absolute cross-section of the scattering process. With a rotating anode of 12 kW, this allows measurement during 6 h only with an excellent signal to noise ratio.

III. THEORY AND CALCULATIONS

A. Osmotic pressure equilibration under external compression forces

In this part we provide the general relationship between the density profile resulting under a constant external force in equilibrium with the repulsive colloidal forces, and the osmotic compressibility. Acting as an external force there could be either the force under rotation in an analytical centrifugation experiment, or simple gravitational force in a sedimentation experiment. The latter is the case for our particles at equilibrations below 1000 Pa, where particles sediment, see Fig. 1(c).

In either case, the dominating force, which counterbalances the colloidal interactions and compresses the sample, is a constant gravitational force. The expected density profile $\rho(z)$ is analog to an atmosphere, i.e. there is an exponential thinning of the colloid density with a typical decay length λ

$$\rho(z) = \rho(0)e^{-z/\lambda}, \text{ with } \lambda = \frac{kT}{\Delta\mu\left(\frac{4\pi}{3}R_p^3\right)g} \tag{3}$$

where $\Delta\mu$ is the mass density of silica minus that of water and z the height coordinate. This profile is obtained from the

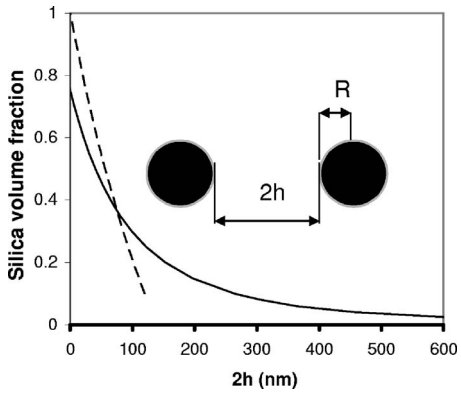

FIG. 2. Volume fraction vs. interstitial distance $2h=\langle H\rangle$ used for the calculation of the interstitial distance, comparing the two approximations: The dashed line corresponds to the "concentrated" regime, while the continuous line corresponds to the diluted regime.

balance between gravitational force and thermodynamic force (osmotic pressure gradient)

$$\rho mg = \rho\Delta\mu\left(\frac{4\pi}{3}R_p^3\right)g = -\left(\frac{\partial\Pi}{\partial z}\right) = -\left(\frac{\partial\Pi}{\partial\rho}\right)\left(\frac{\partial\rho}{dz}\right) \equiv -\frac{kT}{S(0)}\left(\frac{\partial\rho}{dz}\right), \tag{4}$$

where m is the buoyant mass, ρ the particle volume density, and $S(0)$ is the structure factor at $q=0$. It further follows that

$$\frac{\partial \ln \rho(z)}{\partial z} = -\frac{\chi}{\lambda}, \tag{5}$$

where $\chi=kT(\partial\rho/\partial\Pi)$ is the reduced osmotic compressibility, calculated from the equation of state $\Pi(\rho)$ and λ is the decay length, see Eq. (3). Equation (4) also recalls that the osmotic compressibility and the sedimentation profile are completely determined by the *pair* correlations between colloids through the structure factor at origin, $S(0)$ [34]. Thus, sedimentation profiles or density profiles in centrifugation provide information about colloidal interactions via the osmotic compressibility term, if a local particle density gradient is determined with sufficient precision.

B. Conversion of water content into average distance

Two different geometrical cases are considered for the conversion of the water content into an average interstitial distance $\langle H\rangle=2h$ (see Fig. 2):

(1) In the dilute case of silica particle volume fractions Φ below 30%, each silica sphere is considered at the center of a cubic lattice, and the assumption of a hexagonal close random packing leads to the following approximation [24]: The Wigner cell associated to the packing has a volume of $7.66l^3$, where l is the edge of the polyhedron. Then, the volume fraction of the silica particles Φ in such a packing is given by [35]

$$\Phi = \frac{\frac{4}{3}\pi R^3}{7.66l^3} = \frac{3}{4}\frac{R^3}{(R+h)^3}, \tag{6a}$$

resulting in

$$h = R\frac{\left(1-\sqrt[3]{\frac{4\Phi}{3}}\right)}{\sqrt[3]{\frac{4\Phi}{3}}}, \tag{6b}$$

where h is half the average distance between two silica particle surfaces, and R is the silica particle radius, which is determined to be 140 nm (see USAXS data).

(2) In the concentrated case, the interparticle water film is considered as a layer of thickness $2h$, much smaller than the polydispersity of spheres: hence a foamlike structure of connected locally flat water domains with the topology of a dodecahedron is considered. The calculation of the silica volume fraction Φ is performed using the approximation of a dodecahedron [35]

$$\Phi = 1 - \frac{3h}{R+h}. \tag{7a}$$

Then

$$h = R\frac{(1-\Phi)}{(2+\Phi)}, \tag{7b}$$

where R is also the radius of the average foam cell.

The relation between the average distance and volume fraction of silica is given in Fig. 2 in the concentration range typically explored in this study, i.e.. between 70% and 4% silica volume fraction. The equation of state is thus obtained as a plot of the osmotic pressure in dependence of the interstitial distance.

C. Derivation of the compression modulus of PEM material

The isothermal compressibility K_T is given by

$$K_T = -\frac{1}{\phi}\left(\frac{\partial\phi}{\partial\Pi}\right)_T \tag{8}$$

with ϕ as the volume fraction of PEM and water between cores and Π the osmotic pressure. Taking the expression of volume fraction as in Eq. (7a), it is

$$\frac{\partial\phi}{\phi} = \frac{1}{R+h}\partial h. \tag{9a}$$

Hence, if the osmotic pressure is represented by an exponential law, as in Eq. (3), with a contact value Π_0 and a decay length d, it is

$$(K_T)^{-1} = \frac{-1}{R+h}\left(\frac{\partial h}{\partial\Pi}\right)_T = \frac{d}{2\Pi_0(R+h)}e^{-2h/d}. \tag{9b}$$

At contact, h vanishes to zero and the compression modulus in Pa is obtained

$$(K_T)^{-1} = \frac{2\Pi_0 R}{d}. \quad (10)$$

IV. RESULTS

Silica particles are coated with 6–7 layers of polyelectrolytes of alternating charge, yielding multilayers, which are terminated by (PSS) or a polycation, respectively.

Osmotic pressure is imposed onto the dispersions using the dialysis or the vapor pressure method, respectively. A regime of very low pressure can be extracted by letting the dispersion sediment at pressures below about 1000 Pa. Here, the dispersions settle under the influence of gravity, as shown for example for a pressure of zero in Fig. 1(c).

A. USAXS measurements

It is essential to monitor the structure of compressed colloidal dispersions, since coagulation is a known problem in the preparation of polyelectrolyte multilayer- coated colloids. The preparation is typically performed in very dilute dispersions (<1%). Dispersions of PEM-coated colloids have so far not been characterized at high volume fractions. A USAXS study is employed here to monitor colloidal stability and to extract geometrical constants.

In Fig. 3(a) the scattering of the dilute dispersion without compression is shown after desmearing using routine procedures [36]. Oscillations at high q= give direct access to the mass-averaged size of the initial silica particles. From a fit employing the position of minima in the form factor for spherical particles, the radius is deduced as r=140 nm. This value is used in all further calculations. This experiment demonstrates that the coated colloids are well dispersed with a narrow size distribution. Typically four or five oscillations are seen, characteristic for a polydispersity of 5–10 % in radius. Since the polydispersity is relatively small, the water layer film thickness between particles can be considered as an average value over the whole sample. However, the polydispersity is larger than the condensed layer thickness of polymers, so it is justified to employ a foam geometry approximation in order to calculate $\langle H \rangle$ at higher volume fractions (see supporting information).

From the structure factor extracted from x-ray scattering curves, in principle the spacing of particles could be extracted. Figure 3(b) gives USAXS curves of samples equilibrated with solutions of 8% and 12% dextran, respectively, corresponding to osmotic pressures of $\log(\pi/\mathrm{Pa})$=5.0 and 5.4, respectively. At low q values, deviations from the broken curves indicate a structure peak, which arises from the interference between neighboring particles. For the lower curve, obtained at higher osmotic pressure, the structure peak is shifted towards larger q, while the minima originating from the form factor remain at identical q values. Thus, compression leads to a reduced average distance of particles, but not to important shape changes as could be induced by coagulation. The particles are densely packed, but not crystallized, since higher order structure peaks are not observed. Well-dispersed colloidal samples are a prerequisite for meaningful

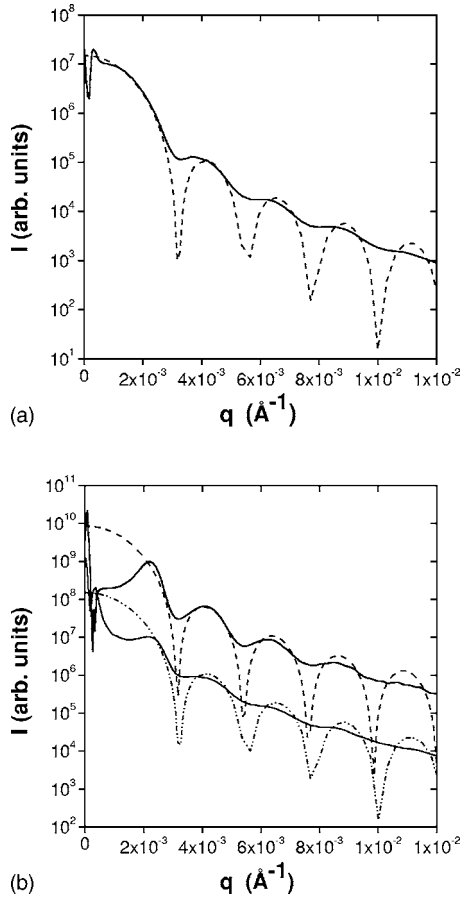

FIG. 3. Scattering curves of dispersions (a) before and (b) after osmotic compression. Full lines: scattering curves after de-smearing of instrumental effects. Broken lines: form factor extracted with a model of monodisperse spheres. (b) Upper lines: compression with 8% dextran solution, lower lines: compression with 12% dextran solution, the latter curves were divided by a factor of 57 in intensity.

osmotic compression experiments. Micro phase separation can be detected by USAXS, since coexistence of two phases in one sample induces a dominating q^{-3} to q^{-4} dependence of the scattering intensity at low q [37,38], which was not observed here.

From the structure peak, the most probable distance between centers of neighboring colloids can be found from the Bragg relation. In principle, an extraction of the average interstitial distance $\langle H \rangle$ is possible. However, the structure maximum starts to overlap with the form factor minimum at q=0,003 Å^{-1} as the pressure increases. Therefore, it turned out that this procedure is not precise enough for application to a large range of volume fractions. Instead, the average interstitial distance was calculated from the water content of the samples.

B. Pressure-distance dependence

From equilibrated samples the water content is determined by Karl Fischer titration or by density methods—depending on the water content—and converted into an average distance between neighboring particles $\langle H \rangle$=2 h, as

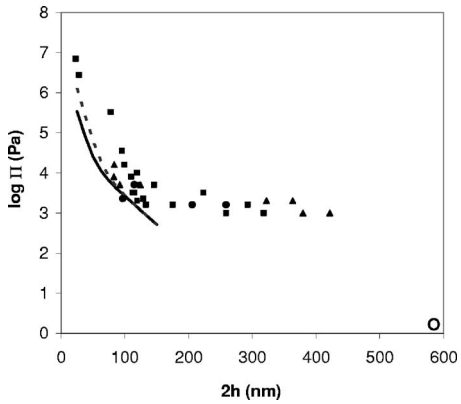

FIG. 4. Equation of state log Π against 2 h for multilayer-coated colloids: (squares) 6 layers, terminated by PAH; (triangles) 6 layers, terminated by PDADMAC; (circles) 7 layers, terminated by PSS; (open symbol) data point obtained for a sedimented sample (see text); (lines) surface force data of [22] converted into pressure data by integration for four layers (full curve) and three layers (dashed curve).

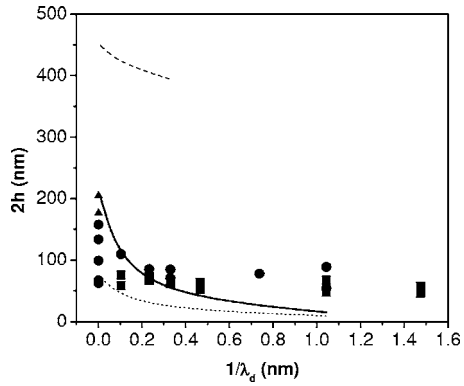

FIG. 5. Particle distance in dependence on the inverse Debye screening length at constant osmotic pressure. Samples were equilibrated at $\log(\Pi/\mathrm{Pa})=3.2$, with varying concentrations of NaCl. Squares: 6 layers, terminated by PAH, triangles: 6 layers, terminated by PDADMAC, and circles: 7 layers, terminated by PSS. The lines correspond to PB theories with different volume distributions of charged monomers. Dotted line: a total charge is collapsed on the capsule surface. Dashed line: a total chargeis distributed in volume in a brush of thickness 200 nm around the capsule. Solid line: an adjusted total charge is distributed in volume on a brush of thickness 200 nm around the capsule.

described in the calculations. The equation of state is thus obtained as a plot of the osmotic pressure versus surface-surface separation. Fig. 4 gives the equation of state as a semi-logarithmic representation of the pressure-distance dependence for compressed dispersions.

Data points are not primarily different when different cationic or anionic polyelectrolytes are used as the last layer. Therefore, the sign of charge or the persistence length of the polyelectrolyte forming the terminating layer does not influence the equation of state.

Three separate regimes can be clearly distinguished: At small distances, a strong repulsion is present, leading to a large slope of the pressure. At particle distances of $2\,h \approx 100$ nm, a distinct transition occurs towards a regime with a very small slope, almost forming a plateau, the origin of which will be discussed below. Finally, a third regime is observed, where the pressure steeply drops at very large distances, as can be seen on the data point at about 600 nm. Also remarkable are the large distances at which the respective crossover points between regimes occur, and the extension of the second regime to very large distances, which will be discussed below.

We note that below a critical osmotic pressure samples sedimented. The data point represented by open symbol in Fig. 4 was obtained from a sedimented sample and was calculated as follows: The average particle density $\langle\rho\rangle$ of the sediment of height $d \approx 3$ mm in equilibrium at $\pi=0$ in the reservoir has been determined and the osmotic pressure at the bottom of the sample obtained from $\pi=m\,g\langle\rho\rangle d \approx 1$ Pa (m: buoyant mass of a particle). The local density at the bottom has been approximated with $\langle\rho\rangle$ and converted into the interstitial distance h value, $2\,\mathrm{h} \approx 600$ nm.

C. Variation of salt concentration at constant pressure

In order to assess the contributions of electrostatic or steric interactions to the osmotic pressure, equilibration experiments were performed in dependence on the Debye screening length, λ_D by using several imposed salt (NaCl) concentration in the dialysis reservoir. Figure 5 gives distance values obtained for $\log(\Pi/\mathrm{Pa})=3.2$ for samples of different salt content (NaCl). The value of $\log(\Pi/\mathrm{Pa})=3.2$ was chosen to be well in the second regime, within the apparent plateau. Note that the membrane used for equilibration is permeable to salt, such that the NaCl does not directly contribute to the osmotic pressure, but only indirectly by a modification of the colloidal interactions.

As the results indicate, the equilibrium distance in the presence of salt is not very sensitive to salt concentration: With a decreasing Debye length λ_D only a slight decrease of the distance might be present. This is evidence that electrostatic forces between separated objects, such as for example double layer repulsion, do not dominate the second regime. Instead, the governing forces are almost independent on λ_D.

V. DISCUSSION AND SIMULATIONS

A. Comparison between osmotic stress and local methods

The osmotic stress technique directly determines the osmotic pressure of a bulk sample. However, since osmotic stress data might depend on the efficiency of the membrane chosen in the low pressure regime, or on the establishment of thermodynamic equilibrium when saturated salts are used [31], it is useful to compare results obtained not in the bulk, but with a closely related chemical situation, i.e. with local studies of layers at a surface. Using the "colloidal probe" atomic force microscopy (AFM) technique ensures that the geometry is controlled at a colloidal scale; alternatively the surface force apparatus (SFA) provides a defined situation of two surfaces in local contact. A differentiation of the energy per unit surface in the Derjaguin regime can be compared to

pressure [23]. Osmotic stress imposed via vapor or via polymers typically extends over seven orders of magnitude from 10^9 to 100 Pa, while three orders of magnitude at best can be obtained via SFA, due to the mechanical properties of springs and glues.

In a recent paper, interactions between planar surfaces coated with four and five layers of PAH/PSS on mica surfaces were investigated by SFA by Blomberg *et al.* [22]. SFA gives as an experimental result the force divided by cylinder radius F/R (N/m) versus separation between supporting surfaces. The osmotic stress method gives the free energy cost/gain associated to removing solvent from the sample. The result is expressed in terms of pressure versus distance in N/m^2. SFA experiments can be converted to osmotic stress data by a procedure described by Parsegian [39], employing a derivation versus the distance, a procedure which has been tested extensively, for the first time for charged bilayers [23]. Here, we follow this procedure to compare the SFA data to our equation of state in the regime of small particle separations, where the colloid geometry is approximated by thin planar water layers with the topology of a "foam" between the particles and the distance h is calculated according to Eq. (7b). First, the data of F/R by Blomberg *et al.* are fitted by a phenomenological biexponential function, which is then derived versus distance: The Derjaguin approximation [40] relates the force measurements in the geometry of crossed cylinders to the energy per surface area between parallel surfaces, E_s, by

$$F(d) = 2\pi R E_s(d). \tag{11}$$

A derivative of the energy per surface area, is then employed to obtain the osmotic pressure in N/m^2.

As can be seen in Fig. 4, after conversion of the SFA data of Blomberg *et al.* into pressure-distance data, the SFA results are similar in the range where both methods are applicable, if bearing in mind that the number of layers was lower in the SFA experiment, which shifts the curves to lower distances.

The three regimes of interactions of PEM-covered particles, which apparently exist in Figure 4, will be discussed in the following and compared to general theoretical models. The physical origin of these three regimes and the information that can be gained is demonstrated.

B. The first regime: Layer deformation

In the range from 10^7 to 4000 Pa, the pressure decreases steeply with the average interparticle distance. It can be phenomenologically described by an exponential law

$$\Pi(H) = \Pi_0 e^{-H/d}. \tag{12}$$

The decay length d is extracted from a fit of the data in this regime, shown as a thick solid line in Fig. 6, and results in $d=12$ nm, while the contact value of the pressure is estimated to 500 atm.

This regime extends up to about 120 nm interparticle distance, which is larger than twice the PEM layer thickness extracted from optical methods for the present preparation conditions, which is about 10 nm [30]; however, the optical

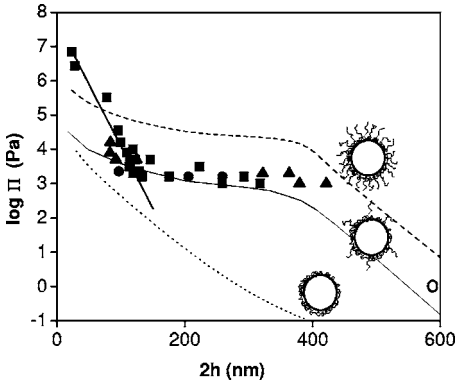

FIG. 6. Equation of state log Π against 2 h for multilayer-coated colloids. The straight line at small distance is a fit as described in the text for the compression regime. The other lines correspond to PB theories with different geometries for the charged monomer distribution. Dotted line: a total charge is collapsed on the particle surface. Dashed line: a total charge is distributed in volume in a brush of layer thickness 200 nm forming a corona around the particle. Solid line: an adjusted total charge is distributed in volume on a brush of thickness 200 nm.

methods rely on a contrast in refractive index, which defines the interface between layers and water at fairly large polymer segment density and does not account for loops and tails extending far out from the condensed layers.

Above a threshold value of 10^7 Pa, the existence of a water film between particle surfaces is limited by formation of air bubbles and capillary condensation at the scale of interstitial bubbles with a curvature of the order of 15 nm^{-1} (core radius/10). Therefore, experiments were not extended to higher pressures.

In the first regime, the compressibility increases suddenly at the turnover point from a regime of compression of the expanding outer layer only to a compression of all layers, the inner condensed ones and the outer one. The experimental result is an increase in compression modulus. The slope of the pressure versus distance curve gives the compression modulus of the PEM as a whole. Employing Eq. (10), the numerical value of the compression modulus at contact is 1 GPa and the minimum value at the threshold of deformation is of the order of 100 kPa. The maximum value can be compared to elasticity moduli determined on hollow PEM capsules: Colloidal probe AFM resulted in 1–2 GPa for larger deformations [20], while osmotically induced capsule deformations led to about 500–750 MPa [41], agreeing well with our maximum for short distances.

C. The second regime: Brush swelling

In the regime between pressures of 1000 and 4000 Pa, the pressure shows a surprisingly weak decrease, corresponding to a high compressibility in this plateau region. We will finally attribute this to the terminating layer extending in a brushlike conformation, but we first discuss limiting straightforward models for interactions that might govern the pressure.

For charged surfaces at large distances, repulsive forces between the respective electric double layers typically domi-

nate the repulsion. As a first approach, calculations were performed assuming hard spheres with charges localized on the surface of the outermost polyelectrolyte layer, at a radius R_p of (140+10) nm=150 nm.

The surface charge of the PEMs can be estimated from the results of the chemical analysis, where the carbon to silica mass ratio is $m_C/m_{Si}=0.09$. We denote as "structural charge" the number of ionizable groups of either polyelectrolyte. Assuming a 1:1 stoichiometry of the structural charges in subsequent layers and taking into account the molecular weights of PAH and PSS results in a polymer coverage of 3.6 mg/m^2 for each bilayer, a value which is in fair agreement with quantitative adsorption studies of polyelectrolytes [42]. Assuming furthermore for the terminating layer that about half of the charged groups are not compensated by the previous layer and thus contribute to the net surface charge σ, then it is $\sigma=7$ μmol/m^2, which corresponds to $Z=1.2\times10^6$ charges per colloid.

A standard non-linearized Poisson-Boltzmann (PB) calculation in the spherical cell geometry has been performed for these size/charge parameters at different volume fractions or cell radii R_{cell} (h is identified with R_{cell}-R_p). The salinity in the reservoir is estimated as 10^{-4} M. This model underestimates the experimental pressures (dotted curve in Fig. 6) and is unable to exhibit a plateau.

However, for this calculation a radius of 150 nm was assumed on the basis of a layer thickness of 10 nm for six layers. While this thickness is reasonable for densely packed multilayers, the terminating layer can be far more extended due to the self-repulsion of the chain. Since the contour lengths of PSS, PAH and PDADMAC are about 90, 220, and 340 nm, respectively, loops and tails can extend far into the aqueous phase, such that their repulsion dominates the particle interaction. Such an enhanced extension, or swelling, is indeed likely to occur, as the PEM formation is performed under the influence of salt, while the osmotic stress equilibration is performed in the absence of additional salt, such that the loops and tails of the terminating layer are experiencing a far larger Debye length.

So, in a second step, we have performed PB calculations with "penetrable" conditions between the outer "corona" of each PEM-coated colloid: the monomers are homogeneously distributed in volume, over a layer $L=200$ nm, from $r=R_p$ to $r=R_{max}=R_p+L=350$ nm. The ions may penetrate into this polymer layer and are distributed inside and outside this layer according to the PB theory. In the third regime, $R_{max}<R_{cell}$ or $2\,h>400$ nm, the hairy layers do not overlap. In the second regime, $R_{max}>R_{cell}$, the polymer brushes are compressed by the neighboring particles. The polymer arms must fold up in order to stay inside the cell and the imposed monomer density is modified accordingly. In order to implicitly account for the hidden local ionic condensation in the 2D geometry around each polymer, the total charge per colloid is reduced by the Manning parameter $\xi\approx2.7$ so the particle charge is $Z'=4\times10^5$. The resulting PB pressure is now able to exhibit a plateau in the second regime but overestimates the experimental data (dashed curve in Fig. 6). Since the pressure is given by the ion density at the cell edge and the counter ion profile roughly matches the monomer one in the second regime, it is sufficient to adjust Z' to the value 2×10^5 to obtain a good quantitative agreement in the second regime. Finally, the residual salt concentration has been fixed at 10^{-4} M in order to reproduce the experimental point in the third regime (solid curve in Fig. 6).

The reduction of Z' and thus the order of magnitude of the osmotic pressure can be explained if one assumes that only 5% of the non-complexed half of the segments of the outer layer participate to the outer corona acting as a brush (see Fig. 6). The remaining part of the last outer layer is condensed on the sphere made of the N-1 layers already condensed on the core.

As can be deduced from Fig. 4, the maximum swelling of the outer layer results in the values of 160, 130 and 215 nm for PAH, PSS and PDAMAC, respectively. All other samples with slightly lower pressures were sedimenting. These distances are of the same order of magnitude as the contour lengths calculated for the mean molecular weight, which are 220, 90, and 340 nm, respectively. Thus, whatever the polyelectrolyte considered, the outer layer can swell from a compressed thickness of 60 nm to at most a value on the order of the contour length, before the turnover from the swelling brush to the nonoverlapping regime occurs.

There would be another possibility for explaining the apparent plateau observed: a coexistence of dense and dilute regions, present as two coexisting phases. Even with only repulsive interactions present, a phase separation could occur in cases of ultra soft interactions. Complex phase diagrams have been theoretically determined for star polyelectrolytes [43,44]. In our case, however, the counter ion repulsion is sufficient to explain the apparent plateau without additional contributions to the interaction potential.

D. The third regime: Weak repulsion

The data point at 600 nm in Fig. 6 indicates the presence of a third regime. Sedimentation of the dispersion is the result of the equilibration at pressures below about 1000 Pa. Sedimentation and the formation of a clear supernatant, as shown in Fig. 1(c), reflect equilibrium with the reservoir, which in the case of Fig. 1(c) is pure water, thus no external osmotic pressure is imposed. The dominating force, which counterbalances the colloidal interactions and compresses the sample, is gravity. As can be seen in the photography on Fig. 1(c), an exponential profile expected according to Eq. (3) can not be observed here: From the optical appearance, a well-defined interface separates pure water from a turbid column of colloids. The concentrated phase exhibits a roughly constant density of colloids, with a sharp interface separating it from pure water. This indicates that colloids stay at a roughly constant distance, where the osmotic compressibility starts to increase.

In order to rationalize this observation made at macroscopic scale, we simulate the particle density profile $\rho(z)$ according to Eq. (3) with the decay length determined in the present case to $\lambda=21$ μm. Fig. 7 displays the particle distance against height in the sample. It is evident that the particle distance and thus also the particle density indeed remain almost constant, i.e. are only slightly exponentially decreasing, over a range of centimeters. Finally, at a certain height a

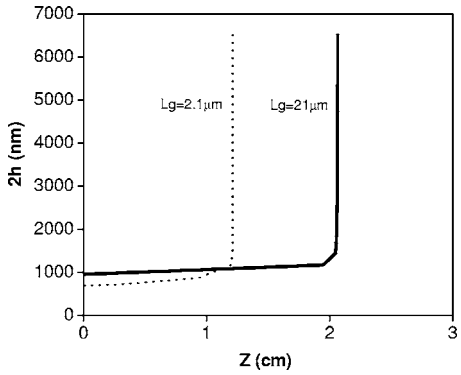

FIG. 7. Theoretical sedimentation profile corresponding to the full line in Fig. 6 for the equation of state. Gravitational length $L_g \equiv \lambda$ equal to 21 μm (corresponding to g) and 2.1 μm at 10 g.

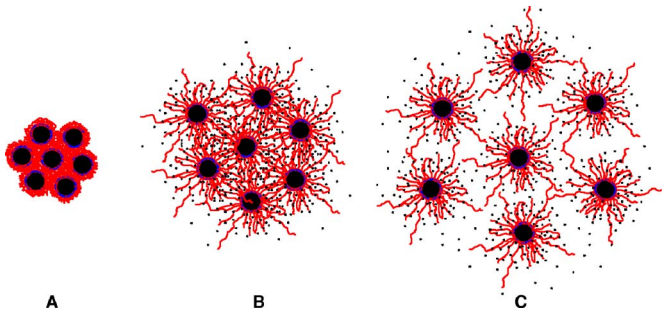

FIG. 8. (Color online) Sketch of interacting particles in the three different regimes, (a) layer deformation, (b) swelling brush, (c) nonoverlapping regime.

sharp increase of distance and a sharp decrease of particle density occur, which is consistent with the observation of a sedimented column of particles. Here, the particles stay at a large distance, where the osmotic compressibility starts to increase.

In this third regime, when a sedimentation layer is present at the bottom of the sample, the osmotic pressure increases quasilinearly between the top and the bottom layer of the sedimented layer. The pressure at equilibrium is of the order of a few Pascal with an interstitial distance between particles of 600 nm. The macroscopic "interface" which appears as smooth to the eye has a typical thickness of less than 0.1 mm, i.e. about five times the gravitation length. In the regime of ultra-weak compression, the thickness as well as the profile within the "interface" between the diluted solution and the sedimented layer could be varied by gentle centrifugation (hand centrifuge, typically g^*10) as demonstrated in principle by the simulation shown in dashed line on Fig. 7. Thus, a hand centrifuge of a z-imaging technique could be turned to a "new" and very sensitive device of weak long-range forces between colloids, typically of the order of Pascals and tenth's of micrometers, as dominated by the outer corona of PEM-covered colloids.

VI. CONCLUSIONS

The physical situation in the three identified regimes is summarized in Fig. 8. To the left, the full multilayer compression regime is shown, when the whole multilayer reacts to strong mechanical stress. In that regime, associated to pressures above 1 atm, a decay length of the repulsion has been determined for the first time by a thermodynamic method. In the second regime [Fig. 8(b)], the gas of noncondensed counter-ions present in the swelling outer layer controls the colloidal interaction. This swelling outer layer is present as an osmotic brush, which contains a small fraction of the polyelectrolyte chains of the terminating layer. This regime continues until somewhat below the contour length of the outer chains.

If less than 1000 Pa of osmotic pressure is applied, the particles sediment and a weak repulsion regime is reached. Here, the pressure can drop over several orders of magnitude along the height of the sample. The particles can be considered as charged hard spheres with an extended, swollen size. There is a sharp meniscus at the top of the two-phase system. Moreover, observation of the variation of the top level of filling versus any small perturbation, such as gentle rotation opens the possibility of a very precise measurement of compressibility of the layer of sedimented swollen particles in this regime.

It is thus demonstrated that employing osmotic pressure, an extremely sensitive method (far better than AFM or SFA) is available. This results in a detailed and generalized method to study colloidal interactions down to very low interaction forces and their response to temperature, dissolved additives, and addition of hydrotropes or non-electrolytes.

ACKNOWLEDGMENTS

Annegret Praast is gratefully acknowledged for performing the multilayer coating of the colloids. This work was funded by the Deutsche Forschungsgemeinschaft within the French-German network "Complex fluids: From 3D to 2D," proposal no. Scho 636/3-1.

[1] J. Perrin, *Les atomes* [Flammarion, 1991 (re-edited)].
[2] H. R. E. Kruyt, *Colloid Science* (Elsevier Press, New York, 1952).
[3] Y. H. Tsao *et al.*, Langmuir **9**, 233 (1993).
[4] R. Podgornik, H. H. Strey, and V. A. Parsegian, *Molecular Interactions in Lipids, DNA, and DNA-lipid Complexes* (Marcel Dekker, Inc., New York, NY, 2000).
[5] L. J. Michot *et al.*, Langmuir **20**, 10829 (2004).
[6] J. Bibette, D. Roux, and B. Pouligny, J. Phys. II **2**, 401 (1992).
[7] F. Ricoul *et al.*, Langmuir **14**, 2645 (1998).
[8] F. Ricoul *et al.*, Eur. Phys. J. B **4**, 333 (1998).
[9] C. B. Stanley and H. H. Strey, Macromolecules **36**(18), 6888 (2003).
[10] G. Holtus, W. Borchard, Colloid Polym. Sci. **267**(12), 1133 (1989).
[11] G. Decher, Science **277**, 1232 (1997).

[12] P. Bertrand *et al.*, Macromol. Rapid Commun. **21**, 319 (2000).
[13] M. Schönhoff, Curr. Opin. Colloid Interface Sci. **8**, 86 (2003).
[14] M. Schönhoff, J. Phys. Condens. Matter **15**, R1781 (2003).
[15] E. Donath *et al.*, Angew. Chem., Int. Ed. **37**, 2202 (1998).
[16] A. A. Antipov *et al.*, J. Phys. Chem. B **105**, 2281 (2001).
[17] X. P. Qiu *et al.*, Langmuir **17**, 5375 (2001).
[18] L. Dähne *et al.*, J. Am. Chem. Soc. **123**, 5431 (2001).
[19] D. Y. Wang, A. L. Rogach, and F. Caruso, Chem. Mater. **15**, 2724 (2003).
[20] F. Dubreuil, N. Elsner, and A. Fery, Eur. Phys. J. E **12**(2), 215 (2000).
[21] K. Lowack and C. A. Helm, Macromolecules **31**, 823 (1998).
[22] E. Blomberg *et al.*, Langmuir **20**, 5432 (2004).
[23] V. A. Parsegian *et al.*, Methods Enzymol. **127**, 400 (1986).
[24] V. Réus *et al.*, J. de Chimie Physique **92**, 1233 (1995).
[25] S. Lyonnard *et al.*, J. Appl. Crystallogr. **33**, 582 (2000).
[26] A. Striolo *et al.*, J. Phys. Chem. B **106**, 5500 (2002).
[27] W. A. Ducker, T. J. Senden, R. M. Pashley, Langmuir **8**(7), 1831 (1992).
[28] P. M. Claesson, T. Ederth, V. Bergeron, M. W. Rutland, Adv. Colloid Interface Sci. **67**, 119 (1996).
[29] G. B. Sukhorukov *et al.*, Colloids Surf., A **137**, 253 (1998).
[30] B. Schwarz and M. Schönhoff, Langmuir **18**, 2964 (2002).
[31] M. Dubois and T. Zemb, J. Phys. IV **8**, 55 (1998).
[32] S. Lyonnard *et al.*, Langmuir **18**, 10386 (2002).
[33] J. Lambard, P. Lesieur, and T. Zemb, J. Phys. I **2**, 1191 (1992).
[34] L. Belloni, J. Chem. Phys. **123**, 204705 (2005).
[35] R. Williams, *The Geometrical Foundation of Natural Structure* (Dover, New York, 1979).
[36] P. Lesieur *et al.*, Physica B **180–181**, 564 (1992).
[37] M. Morvan *et al.*, Colloids Surf., A **82**, 193 (1994).
[38] M. Morvan *et al.*, Langmuir **10**, 2566 (1994).
[39] V. A. Parsegian, R. P. Rand, and N. L. Fuller, J. Phys. Chem. **95**, 4777 (1991).
[40] B. V. Derjaguin, Kolloid-Z. **69**, 155 (1934).
[41] C. Gao *et al.*, Eur. Phys. J. E **5**, 21 (2001).
[42] A. F. Xie and S. Granick, Macromolecules **35**, 1805 (2002).
[43] C. N. Likos *et al.*, J. Phys.: Condens. Matter **15**, S233 (2003).
[44] N. Hoffmann, C. N. Likos, and H. Lowen, J. Chem. Phys. **121**, 7009 (2004).